Loss of Gasdermin D is protective against influenza virus-induced inflammation and mortality

Samuel Speaks[1#], Ashley Zani[1,2#], Abigail Solstad[1], Adam Kenney[1,2], Lizhi Zhang[1,2], Adrian C. Eddy[1,2], Amal O. Amer[1,2], Richard Robinson[1,2], Chuanxi Cai[3], Jianjie Ma[3], Emily A. Hemann[1,2], Adriana Forero[1,2,*] and Jacob S. Yount[1,2,*]

[1]Department of Microbial Infection and Immunity, The Ohio State University, Columbus, OH 43210
[2]Infectious Diseases Institute, The Ohio State University, Columbus, OH 43210
[3]Department of Surgery, Division of Surgical Science, University of Virginia, Charlottesville, VA 22903

[#] Equal Contribution
* Address correspondence to Jacob.Yount@osumc.edu and Adriana.Forero@osumc.edu

Keywords: Gasdermin D, influenza virus, neutrophil, inflammasome

Abstract

Influenza A virus activates cellular inflammasome pathways, though it remains unknown whether many of the effector proteins downstream of inflammasome activation promote virus clearance or instead promote pathological inflammation. We investigated the role of gasdermin D (GSDMD), a pore-forming inflammasome effector protein that allows cellular release of inflammatory molecules and eventual pyroptotic lysis of cells. GSDMD knockout (KO) mice infected with influenza virus exhibited reduced weight loss and mortality compared to infected wild type (WT) mice. Lung viral titers were similar between genotypes, indicating that GSDMD does not directly affect virus replication. Instead, we observed that GSDMD KO mice had less severe lung inflammation, histopathology, and immune cell infiltration, suggesting that GSDMD promotes tissue-damaging immune responses following infection. Global transcriptomic analysis revealed significant decreases in specific inflammatory gene programs in GSDMD KO lungs, including decreased neutrophil chemotaxis and activation gene signatures, which were confirmed by decreased neutrophil elastase measurements and decreased neutrophil numbers in the lung. Indeed, exogenous depletion of neutrophils starting at day 3 post infection in WT mice recapitulated the protective phenotype observed in GSDMD KO mice, implicating neutrophils as central players in the GSDMD-dependent pathological response to influenza virus. Overall, these findings reveal an important role for GSDMD during influenza virus-induced lung inflammation, pathogenesis, and neutrophil accumulation. Therapeutic interventions targeting the GSDMD/neutrophil axis may provide an effective means to treat severe influenza virus infection.

Introduction

Influenza A virus (IAV) infection remains a threat to global public health with seasonal epidemics affecting nearly 10% of the world's population annually and emergent global pandemics remaining an ever-present threat [1,2]. Exuberant inflammatory immune responses and excessive tissue damage often characterize severe IAV infections. Indeed, IAV is known to trigger multiple inflammatory pathways, including the activation of cellular inflammasomes through multiple mechanisms [3]. However, whether inflammasome activation is beneficial or detrimental to the outcome of infection is a topic of debate [4-9]. Further, roles for many of the specific effector proteins downstream of inflammasome activation remain unstudied during influenza virus infection. Here, we exaine the role of Gasdermin D (GSDMD), which is cleaved by inflammasome-activated caspases, allowing it to form cellular pores that release inflammatory products and induce pyroptotic cell death [10-13].

Investigations of the NLRP3 inflammasome revealed that it can be a double-edged sword during influenza virus infection, driving both beneficial antiviral effects and pathological inflammation [3,6]. Knockout of NLRP3 in mice results in accelerated death [5], but partial inhibition of the NLRP3 inflammasome was shown to be beneficial during influenza virus infection [6-8]. Previous work from our lab has also shown that mice treated with an experimental therapeutic protein, recombinant human Mitsugumin 53 (MG53, also known as TRIM72), exhibited dramatically reduced morbidity following otherwise lethal influenza virus infection [14]. MG53 nucleates membrane repair processes and also has anti-inflammatory effects [15]. Indeed, the decreased severity of disease in MG53-treated mice corresponded with significantly lower levels of NLRP3 and IL-1β in the lungs of IAV-infected mice [14]. Interestingly, these treated mice also exhibited reduced levels of activated GSDMD, suggesting to us that excessive inflammasome activation, including GSDMD activity, contributes to pathological inflammation during influenza virus infection.

GSDMD is a member of the pore-forming family of gasdermin proteins, many of which have characterized functions in cell death [8]. Processing of GSDMD involves cleavage of the N-terminal domain from its inhibitory C-terminal domain, allowing the freed N-terminal fragment to assemble into oligomers that stabilize as ring-shaped pores in the plasma membrane [13,16]. Formation of these GSDMD pores allows the release of pro-inflammatory cytokines, such as IL-1β and IL-18 [17-19], which can promote leukocyte recruitment and viral clearance [20,21]. Unresolved pore formation can lead to uncontrolled release of additional inflammatory cytosolic components, pyroptotic cell death, and tissue damage [12,21].

GSDMD has also been associated with the regulation of neutrophil activity and recruitment to inflamed tissues [9,22]. Of the numerous immune cell types important for control of influenza virus infection, neutrophils are among the first to infiltrate sites of infection [23]. Beneficial functions of neutrophils include phagocytic activity, cytokine and chemokine release, and formation of neutrophil extracellular traps (NETs), which are traditionally associated with antibacterial activities but also promote an antiviral state [24-28]. Conversely, other studies have highlighted the potentially detrimental effect of unchecked neutrophil recruitment characterized by hyperinflammation and poor influenza virus-induced disease outcomes in mice, non-human primates, and humans [4,29-32]. Collectively, these observations suggest that neutrophil dynamics may represent a critical determinant of influenza virus pathology. In the present study, we explored the role of GSDMD in IAV infections using GSDMD KO mice and discovered that loss of GSDMD decreases lung inflammation, lung neutrophil accumulation, and mortality during this viral infection. The observed decreases in inflammatory pathology did not affect virus loads or hinder recovery from infection, thus identifying GSDMD as an exciting potential target for decreasing severity of influenza virus infections.

Materials and Methods

THP-1 Cell culture **–** Vector control and and GSDMD KD THP-1 cells were generated by lentiviral shRNA-mediated targeting and were generously provided by Dr. Amal Amer at The Ohio State University. Cells were maintained in RPMI 1640 medium (Fisher scientific) supplemented with 10% EquaFETAL bovine serum (Atlas Biologicals). All cells were cultured in a humidified incubator at 37 °C with 5% CO2. Cells were additionally treated with 25 nM phorbol myristate acetate (PMA) for 3 days as previously described [33] to allow for differentiation into macrophages.

Virus stocks and in vitro infection – Influenza virus A/Puerto Rico/8/34 (H1N1) (PR8, provided by Dr. Thomas Moran of the Icahn School of Medicine at Mt. Sinai) was propagated in embryonated chicken eggs (Charles River Laboratories) and titered as described previously [34]. Infection of THP-1 cells with PR8 was done at an MOI of 10 for 48hrs.

Mouse studies – WT and GSDMD KO mice were purchased from Jackson Laboratories. Mice were infected intranasally under anesthesia with isoflurane according to protocols approved by the Ohio State University Institutional Animal Care and Use Committee. Mouse infections were performed with a dose of 50 TCID50 of PR8. For neutrophil depletion experiments, WT mice

were treated with 0.5 mg anti-mouse Ly6G antibody (InVivoMAb, BE0075-1) or 0.5 mg rat IgG2a isotype control, anti-trinitrophenol antibody (InVivoMAb, BE0089) via intraperitoneal injection on day 3 post infection. From days 4 through 8 post infection, mice were injected with 0.2 mg of the same antibodies. For determining lung titers and cytokine levels, tissues were collected and homogenized in 1ml of PBS, flash-frozen, and stored at −80°C prior to titering on MDCK cells or analysis via ELISA. TCID50 values were calculated using the Reed-Muench method.

Western blotting – For detection of protein expression in lung tissue, samples were lysed in a 1% SDS buffer (1% SDS, 50mM triethanolamine pH 7.4, 150mM NaCl) containing a cocktail of phosphatase protease inhibitors (Sigma, 4906845001) and protease inhibitors (Thermo Scientific, A32965). The lysates were centrifuged at 15,000 rpm for 10 min and soluble protein supernatents were used for Western blot analysis. Equal amounts of protein (30ug) were separated by SDS-PAGE and transferred onto membranes. Membranes were blocked with 10% non-fat milk in Phosphate-buffered saline with 0.1% Tween-20 (PBST) and probed with antibodies against GSDMD (abcam, ab219800) and actin (abcam, ab3280). For Western blotting of THP-1 cells, samples were lysed in 1% SDS containing protease inhibitors prior to SDS-PAGE separation as described above. Membranes were probed with antibodies against influenza virus nucleoprotein (abcam, ab20343), GSDMD (abcam, ab210070), and GAPDH (Thermo Scientific, ZG003).

Single and multiplex ELISAs – human IL-1β, IL-6, CCL1, and TNF, and mouse IFNβ and CCL1 ELISAs were performed on supernatent from lung homogenates or cell culture supernatants using the respective R&D Systems Duoset ELISA kits (catalogue # DY201, DY206, DY8234, DY272, and DY845) according to manufacturer's instructions. Mouse TNF-α, IL-6, and IL-1β levels were also assayed via multiplex ELISA (Mesoscale Diagnostics, mouse V-plex pro-inflammatory panel 1, K15048D) performed by the OSUMC Center for Clinical Research Management core facility.

Flow cytometry – On day 7 post influenza virus infection, mice were euthanized and lungs were homogenized in GentleMACS C tubes (Miltenyi) containing Dnase I (Sigma Aldrich) and type IV collagenase (Worthington Biochemical Corporation). Lungs were processed into single cell suspensions using GentleMACS equipment. Single cell homogenates were blocked in CellBlox (Invitrogen) and viability stain was performed using eFluor 780 Fixable Viability Dye (Invitrogen)

according to the manufacturer's instructions. Cells were washed and stained with Invitrogen antibodies for CD45, Ly6G and Ly6C (catalogue number M001T02R02, 46-9668-82, and 48-5932-82, respectively) for 30 minutes on ice. Cells were fixed with BD FACS lysis buffer for 10 minutes at 4°C, resuspended in PBS, and run on a Cytek Aurora instrument. Count beads (Invitrogen) were added to each sample for quantification of total cell number. Samples were analyzed using FlowJo Software (10.8.1).

Histology – For lung histology (H&E and anti-CD45 staining), lung tissue samples were fixed in 10% neutral-buffered formalin at 4°C for 24 hours and then transferred to 70% ethanol. Lungs were embedded in paraffin, sectioned, stained, and imaged by Histowiz (Histowiz.com, Brooklyn, NY, USA). Unbiased electronic quantification of resultant images was performed using ImageJ software and the color deconvolution method as described previously [9,35-37].

RNA sequencing and Functional Enrichment Analysis **–** RNA was extracted from lung tissue using TRIzol (Invitrogen). RNA library preparation and sequencing was performed by GENEWIZ (GENEWIZ LLC./Azenta US, Inc South Plainfield, NJ, USA) with the following methods, as provided by GENEWIZ: "The RNA samples received were quantified using Qubit 2.0 Fluorometer (ThermoFisher Scientific, Waltham, MA, USA) and RNA integrity was checked using TapeStation (Agilent Technologies, Palo Alto, CA, USA). The RNA sequencing libraries were prepared using the NEBNext Ultra II RNA Library Prep Kit for Illumina using manufacturer's instructions (New England Biolabs, Ipswich, MA, USA). Briefly, mRNAs were initially enriched with Oligod(T) beads. Enriched mRNAs were fragmented for 15 minutes at 94 °C. First strand and second strand cDNA were subsequently synthesized. cDNA fragments were end repaired and adenylated at 3'ends, and universal adapters were ligated to cDNA fragments, followed by index addition and library enrichment by PCR with limited cycles. The sequencing libraries were validated on the Agilent TapeStation (Agilent Technologies, Palo Alto, CA, USA), and quantified by using Qubit 2.0 Fluorometer (ThermoFisher Scientific, Waltham, MA, USA) as well as by quantitative PCR (KAPA Biosystems, Wilmington, MA, USA). The sequencing libraries were multiplexed and clustered onto a flowcell. After clustering, the flowcell was loaded onto the Illumina HiSeq instrument according to manufacturer's instructions. The samples were sequenced using a 2x150bp Paired End (PE) configuration. Image analysis and base calling were conducted by the HiSeq Control Software (HCS). Raw sequence data (.bcl files) generated from Illumina HiSeq was converted into fastq files and de-multiplexed using Illumina bcl2fastq 2.17 software. One mis-match was allowed for index sequence identification."

Raw fastq files were processed, aligned and quantified with a HyperScale architecture developed by ROSALIND (ROSALIND, Inc. San Diego, CA, https://rosalind.bio/). Read Distribution percentages, violin plots, identity heatmaps, and sample MDS plots were generated as part of the quality control step. Statistical analysis for differential gene expression was performed using the "limma" R library [38]. The principal component analysis and volcano plots were formatted in PRISM software using numerical values provided by ROSALIND. Heatmaps were generated from gene expression values provided by ROSALIND using Morpheus software. The topGO R library was used to determine local similarities and dependencies between GO terms in order to perform Elim pruning correction. Additional analysis was performed using the REACTOME database [39], PanglaoDB [40], and Ingenuity Pathway Analysis (Qiagen).

Results

GSDMD potentiates inflammatory responses and morbidity during severe influenza virus infection in mice

To investigate the roles of GSDMD during influenza virus infection, we infected wild type (WT) and GSDMD KO mice with influenza virus strain A/Puerto Rico/8/34 (H1N1) (referred to hereafter as PR8). We first examined lungs for total GSDMD levels, as well as cleaved GSDMD N-terminal fragment indicative of activation, at day 7 post infection via western blotting. Cleaved GSDMD was detected in the lungs of infected WT mice as expected [14], whereas only full-length GSDMD could be seen in lungs from mock-infected WT mice (**Fig 1A**). GSDMD could not be detected in lungs from infected GSDMD KO mice, confirming the expected lack of GSDMD protein in these animals (**Fig 1A**). GSDMD KO mice also lost significantly less weight than their WT counterparts starting on day 5 post infection and continuing through day 7 (**Fig 1B**). The observed weight loss difference may actually underestimate the protective effects of GSDMD deficiency because WT mice had significantly higher mortality rates throughout infection; thus, the sickest animals were removed from the study as they succumbed to infection, skewing the subsequent weight averages. Indeed, over 60% of WT mice succumbed to infection, compared to roughly 10% of GSDMD KO animals, demonstrating a profound protective effect of the loss of GSDMD (**Fig 1C**).

Additional mice were sacrificed on day 7 post infection for analysis of viral titers and inflammatory cytokine levels in the lungs. Virus titers in the lungs of WT and KO mice were similar (**Fig 1D**), indicating that GSDMD increases the severity of influenza virus infection without directly affecting virus replication. Indeed, GSDMD KO mice on average had decreased

levels of pro-inflammatory cytokines such as IL-6 and IFNβ, with levels of TNFα showing a statistically significant decrease compared to WT mice (**Fig 1E**). Interestingly, levels of IL-1β varied widely between animals and did not correlate with animal genotype despite the established role of GSDMD in facilitating release of IL-1β [17-19] (**Fig 1E**). This is consistent with our previous findings in which GSDMD was required for maximal levels of IL-1β in the lung early in SARS-CoV-2 infection, but was dispensible later in infection [9]. We also observed that the chemokine CCL1 was significantly decreased in GSDMD KO lungs compared to WT, consistent with the reported role for GSDMD in immune cell chemotaxis [41,42] (**Fig 1E**).

To determine whether human GSDMD functions similarly to its mouse counterpart in promoting cytokine and chemokine secretion during influenza virus infection, we infected WT and GSDMD knockdown (KD) human THP1 macrophages and measured viral protein and cytokine levels after 48 hours. Consistent with known functions of GSDMD and our *in vivo* results, we saw a large decrease in IL-1β, IL-6, IFNβ and CCL1 levels secreted by GSDMD KD macrophages despite comparable levels of infection as indicated by detection of by viral nucleoprotein expression by Western blotting (**Supplemental Figure 1A-C**). Collectively, our results demonstrate that loss of GSDMD protects against severe influenza virus-induced illness without affecting lung virus loads. Likewise, GSDMD broadly promotes release of inflammatory mediators in both mouse and human cells during influenza virus infections.

GSDMD facilitates immune cell recruitment to the lungs during IAV infection

Given our results indicating decreased cytokine and chemokine secretion in GSDMD KO lungs, we hypothesized that lack of GSDMD leads to decreased inflammatory pathology following influenza virus infection. Thus, we examined gross lung pathology via hematoxylin and eosin (H&E) staining of lung sections at day 7 post infection. Although all infected lung sections showed areas of cell infiltration and consolidation, WT lungs had more severe pathology with immensely thickened alveolar septa, extensive macrophage, neutrophil, and lymphocyte accumulation, and less open airspace (**Fig 2A**). Areas of cellular consolidation versus open airspace were quantified to determine relative lung cellularity as a measure of pathology in individual mice [9,36]. GSDMD KO mice showed decreased lung pathology via this unbiased quantification method as compared to WT mice (**Fig 2B**).

We next stained for the hematopoietic immune cell marker CD45 in lung sections to assess whether the decreased cellularity/consolidation that we observed in GSDMD KO versus WT lungs was due to dampened immune cell infiltration. We observed that infected GSDMD KO mouse lungs contained fewer $CD45^+$ immune cells throughout their lung sections when

compared to infected WT lungs (**Fig 3A**). Notably, immune cells were often clustered around the peribronchole and perivascular spaces in WT mice compared to more diffuse immune cell staining through the lung tissue of GSDMD KO mice. Quantification of CD45 staining of lung sections from individual mice confirmed a significant decrease in $CD45^+$ cells in GSDMD KO relative to WT lungs (**Fig 3B**). These results indicate that loss of GSDMD decreases immune cell recruitment to the lung and limits immune-mediated pathology during influenza virus infection, consistent with our observed protection of GSDMD KO mice from influenza virus-induced morbidity and mortality.

GSDMD KO mice have altered transcriptional responses following influenza virus infection

To further understand the underlying mechanisms contributing to differences in survival and lung damage between WT and GSDMD KO animals, we compared global gene transcriptional responses of WT and GSDMD KO mice following influenza virus infection. Quantitative measurement of total mRNA expression from infected lungs at day 7 post infection showed distinct gene expression programs elicited between WT and GSDMD KO animals as as revealed by principal components analysis (**Fig 4A**). Statistical analysis of differential gene expression (fold change |3|, p-adj < 0.01) captured 812 genes that were increased in infected WT mice compared to infected GSDMD KO mice, while expression of 447 genes was increased in KOs, for a total of 1259 differentially expressed genes (**Fig 4B,C**). Gene set enrichment analysis reproducibly identified significant changes in antiviral immune responses between WT and GSDMD KO mice (**Fig 4D**). Notably, pathways associated with inflammatory defense responses to virus infection were decreased in GSDMD KO lungs. This gene set included interferons (IFNs), IFN-stimulated chemokines, and classical antiviral IFN-stimulated genes such as MX and OAS family genes (**Fig 4E**). These results are in accord with reports that the canonical GSDMD-dependent cytokine IL-1β can amplify the IFN response via induction of IRF1 [43,44], which was also decreased in GSDMD KO mice (**Fig 4E**). In agreement with our ELISA data (**Fig 1E**), our RNAseq analyses revealed an attenuation of inflammatory cytokine and chemokine gene programs in GSDMD KO lungs in general, with CCL1, a chemokine secreted by activated monocytes, macrophages, and T cells, being the most significantly downregulated gene identified (**Fig 4D**). Together with our viral titer and ELISA measurements, these gene expression data collectively suggest that dampened inflammatory responses in the absence of GSDMD underly the decreased lung pathology and increased survival of GSDMD KO mice following influenza virus infection.

Loss of GSDMD results in decreased neutrophil recruitment to lungs during influenza virus infection

In addition to changes in cytokines and chemokines, functional enrichment analysis of differentially expressed genes that intersect with immune cell specific gene expression (PanglaoDB) suggested significant decreases in myeloid cells in GSDMD KO lungs (**Fig 5A**). This was consistent with observed enrichment of biological pathways involved in granulocytic neutrophil function (**Fig 4D**). This included changes in genes associated with neutrophil degranulation (**Fig 5B**) as well as decreases in genes for chemokines that recruit neutrophils, chemokine receptors expressed on neutrophils, and other molecules associated with neutrophil function (**Fig 5C**). Thus, we examined whether GSDMD was involved in neutrophil recruitment to the lungs during influenza virus infection. We found that infected WT mice exhibited robust neutrophil recruitment to the lungs at day 7 post infection (**Fig 5D**), while there was no observable increase in neutrophil infiltration in GSDMD KO mice (**Fig 5E**). This was consistent with a decrease in the levels of neutrophil elastase (ELA2), an indicator of activated neutrophils and clinical marker of disease severity [45], in GSDMD KO as compared to WT lungs (**Fig 5F**). These results suggest that GSDMD expression is required for the full recruitment of neutrophils to the lung during influenza virus infection.

To probe whether decreased neutrophil infiltration could explain the decrease in influenza virus infection severity that we observed in the GSDMD KO animals, we depleted neutrophils early in infection of WT mice and measured infection outcomes. Briefly, we treated mice antibodies targeting neutrophils (α-Ly6G) or isotype control antibody, starting at day 3 post infection through day 8 post infection (**Fig 6A**). This treatment timeline was chosen to allow acute neutrophil responses to proceed uninhibited prior to blockade of a presumptive excessive, pathological response. We confirmed that antibody-mediated depletion led to a marked decrease in total neutrophil numbers, as well as relative percentage of neutrophils compared to the entire immune cell population, in the lungs of α-Ly6G treated mice at day 5 post infection (**Fig 6B**). The specificity of neutrophil depletion was further confirmed by analyzing total counts and percentages of eosinophils and alveolar macrophages compared to all $CD45^+$ immune cells, which were not significantly different between the two treatment groups. (**Fig 6B**). When examining morbidity between the cohorts of mice, the α-Ly6G treated mice experienced significantly less influenza virus-induced weight loss than the isotype control treated group (**Fig 6C**). Remarkably, neutrophil depletion was completely protective against lethal infection,

whereas we observed 60% lethality in isotype control-treated mice (**Fig 6D**), a result that mirrored the protective effects seen in GSDMD KO mice.

Also similar to results comparing GSDMD KO and WT mice mice, viral titers in the lungs of neutrophil-depleted and control treated mice were not statistically different from one another at either day 5 or day 7 post infection (**Fig 6E**). We further observed that levels of several inflammatory cytokines, including IL-1β, IL-6, IFNβ and TNF-α, were significantly decreased in the lungs of neutrophil-depleted mice at day 5 post infection (**Fig 6F**). Likewise, CCL1 levels were commensurately decreased following α-Ly6G treatment, suggesting that neutrophils may potentiate a postive-feedback loop of immune cell chemotaxis (**Fig 6F**). Finally, we quantified neutrophil elastase in the lungs of α-Ly6G treated and isotype control treated mice to further confirm that neutrophil elastase serves as a marker of neutrophil presence and activity. Indeed, we saw decreased neutrophil elastase in the lungs of α-Ly6G treated mice, reinforcing our data showing a similar change in GSDMD KO mice with less neutrophil presence (**Fig 5F).** In sum, our results presented here demonstrate that neutrophil recruitment to the lungs during influenza virus infection is largely dependent on GSDMD and that neutrophils contribute to a pathological inflammatory response and influenza mortality.

Discussion

Our results have identified a detrimental role for GSDMD during influenza virus infection. We found that in the absence of GSDMD, mice experienced reduced morbidity and mortality despite viral burden in the lungs being unaffected (**Fig 1**). Without contributing to the control of virus titers, we found that GSDMD profoundly contributed to lung inflammation, immune cell recruitment, and histopathology (**Fig 1-3)**. The improved outcome of GSDMD KO mice following influenza virus infection compared to WT mice corresponded to global transcriptional decreases in a multitude of tissue-damaging inflammatory pathways (**Fig 4**). Additionally, impaired neutrophil chemotaxis and activity gene expression programs in the absence of GSDMD correlated with improved disease outcome, which we subsequently substantiated via exogenous depletion of these immune cells (**Fig 5,6**). These results suggest that overabundant neutrophils drive disease severity in the context of influenza virus infection. Indeed, our data add to a growing number of studies suggesting excessive neutrophil recruitment correlates with poor disease outcomes [29-31].

Importantly, GSDMD was also required for maximal pro-inflammatory cytokine secretion by human macrophages infected with influenza virus, suggesting that human GSDMD likely also drives inflammation in human influenza virus infections (**Supplemental Figure 1**). This paralells

recent data showing GSDMD co-localization with pyroptotic macrophages in the lungs of severely infected macaques, which also had widespread expression of pro-inflammatory cytokines [4]. In addition to providing an important paralles between murine, non-human primate, and human GSDMD, these data suggest that GSDMD also regulates cytokine production/secretion in macrophages, which are known targets of influenza virus infections [46,47].

Influenza virus infection is among the most common causes of acute respiratory distress syndrome (ARDS) in adults [48]. Development of ARDS is marked by bilateral edema and worsened oxygen delivery [49], and a major contributor to these criteria is the unchecked inflammation caused by cellular immune responses activated to control replicating virus. Specifically, neutrophil infiltration and abundance is correlated with the severity of ARDS [50], and neutrophil secretion of tissue damaging enzymes and inflammatory extracellular traps can exacerbate progression of ARDS [48]. Likewise, GSDMD-mediated NETosis was recently identified as a driver of disease progression in an LPS-induced model of ARDS [51]. Given that GSDMD is a broad promoter of inflammation in response to infection and that there are numerous infectious causes of ARDS, our results suggest that GSDMD may be a potential therapeutic target for mitigating ARDS progression in the context of respiratory infections.

While GSDMD is the final effector protein in the pyroptosis pathway, the possibility remains that other intermediate proteins are contributing to the outcome of influenza virus infection. Multiple caspases have been implicated in both positively and negatively regulating infection. Caspase-1 has been shown to exacerbate acute illness but also promote adaptive immunity to influenza virus [52,53], whereas caspase-3 activation during the onset of apoptosis may be crucial for immune antagonism and efficient influenza virus propagation [54,55]. Interplay of these proteins, and whether the overlapping pathways they affect are synergistic or compensatory, remains to be determined.

Our unexpected results indicating that IL-1β levels are unaffected by the absence of GSDMD, despite its canonical role in IL-1β release [17-19], suggest that there there are redundant mechanisms for pyroptotic cytokine release during influenza virus infection, at least at late timepoints following infection. Indeed, these results are in accord with our published findings that IL-1β levels in the lung at day 2 post infection with SARS-CoV-2 are dependent on GSDMD, but that IL-1β release occurs in a GSDMD-independent manner at later times post infection [18]. Interestingly, we found that loss of GSDMD was not beneficial in SARS-CoV-2 infection [9], highlighting intriguing differences in the pathological mechanisms activated by SARS-CoV-2 versus influenza virus that warrant further study. Excitingly, we observed a previously unreported effect of GSDMD in promoting IFNβ expression and production (**Fig 1, 4,**

S1), further suggesting that GSDMD potentiates pro-inflammatory responses beyond release of canonical inflammasome molecules. Interestingly, attenuation of a number of pro-inflammatory cytokine responses, including IFNβ, in GSDMD KO mice had no appreciable effect on virus replication. However, it is well established that the pathological, tissue-damaging effects of IFNs continue to accumulate beyond the point at which their antiviral effects peak [56-58]. These data suggest that GSDMD KO mice mount a blunted, but sufficient, pro-inflammatory response to combat virus replication without developing the severe morbidity associated with cytokine storm.

Overall, we discovered that GSDMD promotes inflammatory lung pathology during influenza virus infection. Importantly, GSDMD is dispensible for virus control, but exacerbates severe illness, thus identifying it as a promising candidate for host-directed therapeutic targeting during influenza virus infection.

Author Contributions

Conceptualization: AOA, CC, JM, JSY; Data Curation: AF, JSY; Formal analysis: SS, AZ, AS, ADK, RR, EAH, AF, JSY; Investigation: SS, AZ, AS, ADK, LZ, ACE, JK, EAH; Visualization: SS, AZ, AS, ADK, AF, JSY; Writing – Original Draft: SS, AZ, ADK, JM, AF, JSY; Supervision: JSY; Project Administration: JSY; Funding Acquisition: JSY; Resources: AOA, CC, JM.

Acknowledgments

Research in the Yount laboratory is supported by NIH Grants AI130110, AI151230, HL154001, HL157215, and an American Lung Association COVID-19 and Emerging Respiratory Viruses Research Award. AZ was supported by an NSF-GRFP fellowship grant. ADK is supported by an institutional T32 postdoctoral fellowship (NIH grant AI165391).

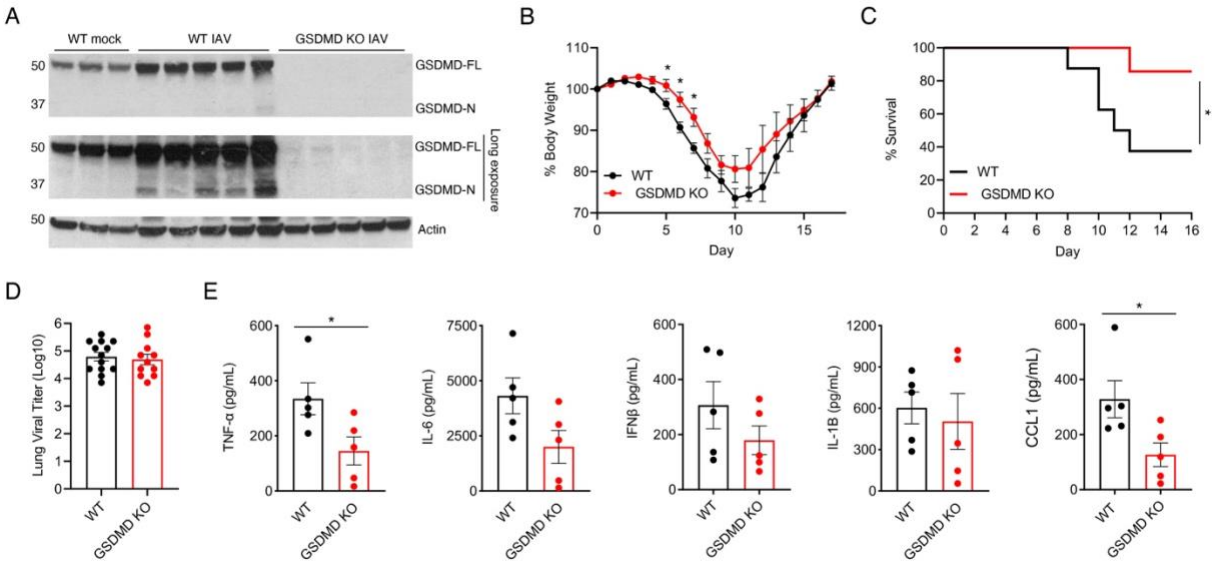

Figure 1: GSDMD promotes inflammation and morbidity following IAV infection. A-I WT and GSDMD KO mice were intranasally infected with 50 TCID50 of PR8. **A** Western blot of lung lysates taken at day 7 post infection. **B** Weight loss (*p < 0.05 Mann-Whitney test) from 3 independent experiments. **C** Survival curve (*p < 0.05 Log-rank (Mantel-Cox) test) from 3 independent experiments. **D** Viral titers from lung homogenates taken at day 7 post infection from 3 independent experiments. **E** ELISA quantification of TNFα, IL-6, IFNβ, IL-1β, or CCL1 levels in lung homogenates of WT and GSDMD KO mice at day 7 post infection. (*p < 0.05, t-test).

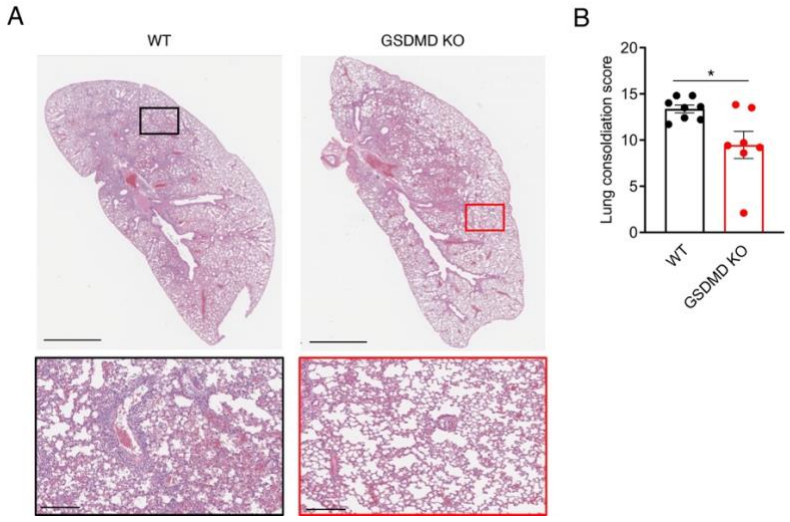

Figure 2: GSDMD exacerbates lung pathology following IAV infection. A Representative H&E images for WT and GSDMD KO mice at day 7 post-infection. Insets show magnified areas of cell infiltration. Scale bars represent 2mm and 200um, respectively. **B** Quantification of H&E staining for entire lung sections of multiple animals in two separate experiments (*p < 0.05, t-test).

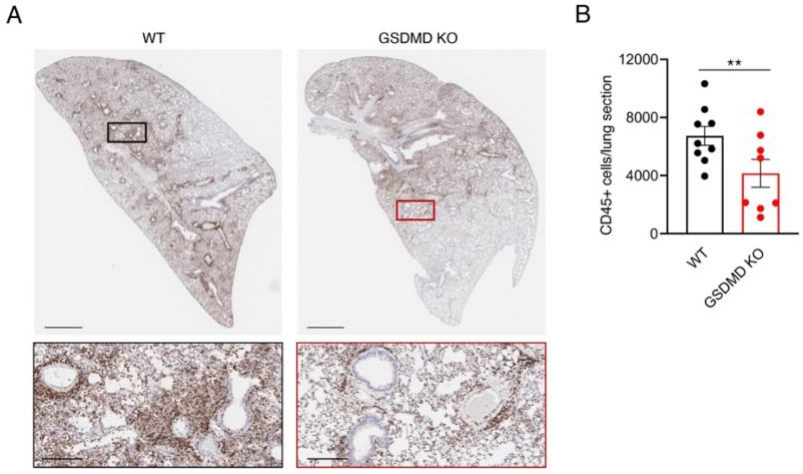

Figure 3: GSDMD deficiency attenuates immune cell infiltration to the lung following IAV infection. A Representative CD45$^+$ IHC images for WT and GSDMD KO mice at day 7 post-infection. Insets show magnified areas of CD45$^+$ immune cell infiltration. Scale bars represent 2mm and 200um, respectively. **B** Quantification of CD45 staining for multiple animals in two separate experiments (** p < 0.01, t-test).

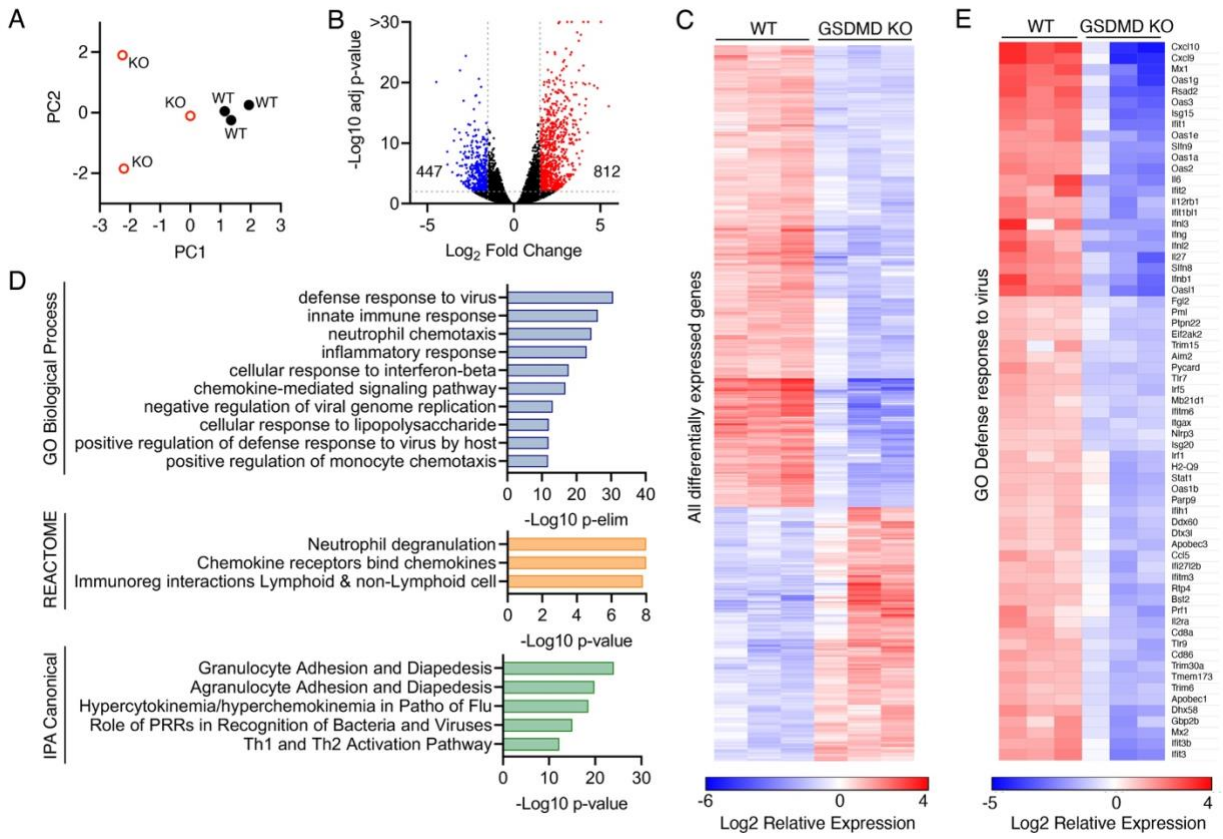

Figure 4: GSDMD is associated with inflammatory gene expression programs. A Principal component analysis comparing WT and GSDMD KO RNA samples. **B** Volcano plot of differential gene expression comparing WT vs GSDMD KO. Purple, 812 genes upregulated in WT vs KO; Green, 447 genes downregulated in WT vs KO. **C** Heat map for top genes that show differential expression between GSDMD KOs and WT **D** Genes decreased in KO versus WT were subjected to pathway and ontology analysis. The top ten most significant GO Biological Processes are shown (-Log10 p-Elim pruning value is graphed) and the significant REACTOME gene set enrichments are shown ($p<0.05$). All differentially expressed genes were examined using Ingenuity Pathway Analysis and the top five most significant Canonical Pathways are shown. **E** Heat map for genes from the top most significant GO Biological Process as shown in **D** (Defense response to virus).

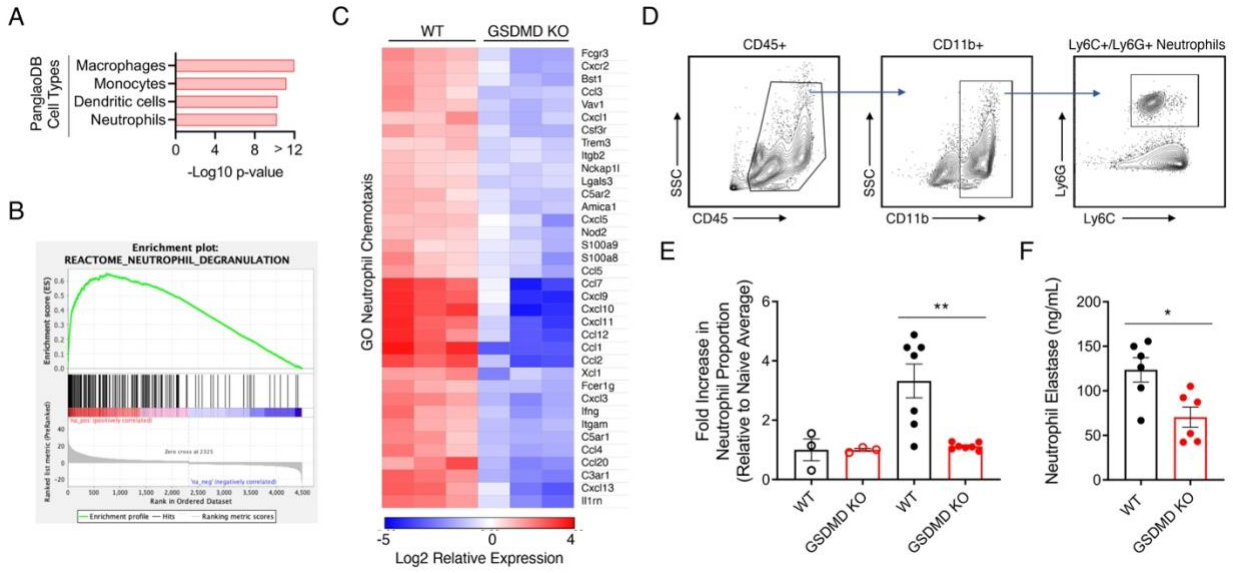

Figure 5: Neutrophil recruitment and chemotaxis is diminished in GSDMD KO mice. A,B RNAseq results as in Figure 4 were further analyzed. A Upregulated genes in WT versus GSDMD KO lungs were subjected to PanglaoDB analysis and all significant associations with specific cell types are shown.**B** REACTOME analysis of differentially expressed genes in WT versus GSDMD KO mice identified significant associations with neutrophil degranulation. **C** Heat map for top differentially regulated genes involved with neutrophil chemotaxis as defined by GO biological processes. **D** Gating strategy to isolate neutrophils from day 7 lung homogenate using flow cytometry. **E** Fold increase in the frequency of neutrophils relative to naïve controls for each group (*p < 0.05, **p<0.01, one-way ANOVA). **F** ELISA quantification of neutrophil elastase levels in lung homogenates of WT and GSDMD KO mice at day 7 post infection. (*p < 0.05, t-test).

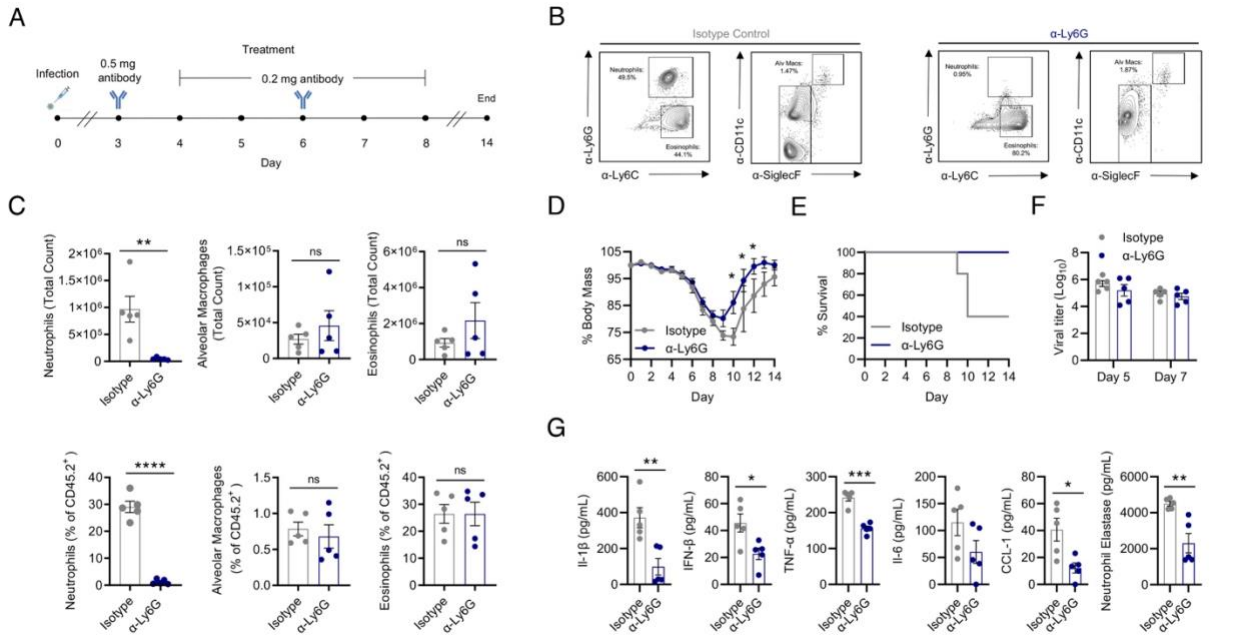

Figure 6: Neutrophils potentiate severe influenza virus-associated illness. A WT mice were infected with 50 TCID50 of PR8. Mice were treated via intraperitoneal (IP) injection with 0.5mg of α-Ly6G antibody or isotype control antibody on day three post infection, followed by 0.2mg of the corresponding antibody on days four through eight. **B** Representative flow cytometry dot plots showing neutrophil, eosinophil, and alveolar macrophage gating of single-cell suspensions from lungs on day 7 post infection. (**p < 0.005, ****p < 0.0001) **C** Neutrophil, eosinophil, and alveolar macrophage total number and percentage of $CD45^+$ cells in the lung on day 5 post infection **D** Weight loss of mice infected as in **A** that were followed until recovery (*p < 0.005, Mann-Whitney test). **E** Survival analysis of mice as infected in **A**. **F** Viral titers from lung homogenates at day 5 and day 7 post infection. **G** ELISAs of pro-inflammatory cytokines performed on lung homogenates from day 7 post infection (*p < 0.05, ** p < 0.01, *** p < 0.001, t-test).

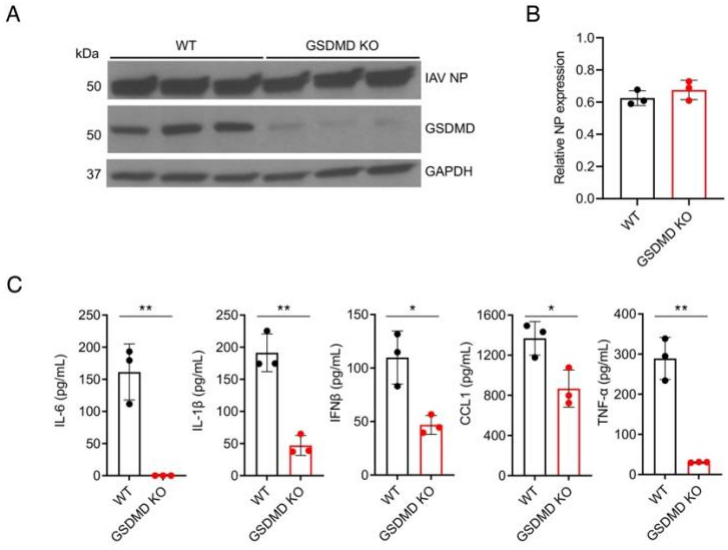

Supplemental Figure 1: Human GSDMD promotes secretion of pro-inflammatory cytokines *in vitro*. A Western blotting for PMA-differentiated WT and GSDMD knockdown human THP1 macrophages 48 hours post infection with PR8 at an MOI of 10 (NP = influenza virus nucleoprotein). Three technical replicates from one experiment were probed. **B** Densitometry quantifaction of NP levels relative to GAPDH in **A**. **C** ELISA quantification of IL-6, IFNβ, IL-1β, CCL1, or TNF-α levels in supernatants from cells infected as in **A** (*p < 0.05, **p < 0.01, t-test).

References

1. Lee, S.S., Viboud, C., and Petersen, E. (2022). Understanding the rebound of influenza in the post COVID-19 pandemic period holds important clues for epidemiology and control. Int J Infect Dis *122*, 1002-1004. 10.1016/j.ijid.2022.08.002.
2. Javanian, M., Barary, M., Ghebrehewet, S., Koppolu, V., Vasigala, V., and Ebrahimpour, S. (2021). A brief review of influenza virus infection. J Med Virol *93*, 4638-4646. 10.1002/jmv.26990.
3. Seveau, S., Turner, J., Gavrilin, M.A., Torrelles, J.B., Hall-Stoodley, L., Yount, J.S., and Amer, A.O. (2018). Checks and Balances between Autophagy and Inflammasomes during Infection. J Mol Biol *430*, 174-192. 10.1016/j.jmb.2017.11.006.
4. Corry, J., Kettenburg, G., Upadhyay, A.A., Wallace, M., Marti, M.M., Wonderlich, E.R., Bissel, S.J., Goss, K., Sturgeon, T.J., Watkins, S.C., et al. (2022). Infiltration of inflammatory macrophages and neutrophils and widespread pyroptosis in lung drive influenza lethality in nonhuman primates. PLoS Pathog *18*, e1010395. 10.1371/journal.ppat.1010395.
5. Allen, I.C., Scull, M.A., Moore, C.B., Holl, E.K., McElvania-TeKippe, E., Taxman, D.J., Guthrie, E.H., Pickles, R.J., and Ting, J.P. (2009). The NLRP3 inflammasome mediates in vivo innate immunity to influenza A virus through recognition of viral RNA. Immunity *30*, 556-565. 10.1016/j.immuni.2009.02.005.
6. Tate, M.D., and Mansell, A. (2018). An update on the NLRP3 inflammasome and influenza: the road to redemption or perdition? Curr Opin Immunol *54*, 80-85. 10.1016/j.coi.2018.06.005.
7. Chung, W.C., Kang, H.R., Yoon, H., Kang, S.J., Ting, J.P., and Song, M.J. (2015). Influenza A Virus NS1 Protein Inhibits the NLRP3 Inflammasome. PLoS One *10*, e0126456. 10.1371/journal.pone.0126456.
8. Kuriakose, T., Man, S.M., Malireddi, R.K., Karki, R., Kesavardhana, S., Place, D.E., Neale, G., Vogel, P., and Kanneganti, T.D. (2016). ZBP1/DAI is an innate sensor of influenza virus triggering the NLRP3 inflammasome and programmed cell death pathways. Sci Immunol *1*. 10.1126/sciimmunol.aag2045.
9. Eltobgy, M.M., Zani, A., Kenney, A.D., Estfanous, S., Kim, E., Badr, A., Carafice, C., Daily, K., Whitham, O., Pietrzak, M., et al. (2022). Caspase-4/11 exacerbates disease severity in SARS-CoV-2 infection by promoting inflammation and immunothrombosis. Proc Natl Acad Sci U S A *119*, e2202012119. 10.1073/pnas.2202012119.
10. Yu, P., Zhang, X., Liu, N., Tang, L., Peng, C., and Chen, X. (2021). Pyroptosis: mechanisms and diseases. Signal Transduct Target Ther *6*, 128. 10.1038/s41392-021-00507-5.
11. Kayagaki, N., Stowe, I.B., Lee, B.L., O'Rourke, K., Anderson, K., Warming, S., Cuellar, T., Haley, B., Roose-Girma, M., Phung, Q.T., et al. (2015). Caspase-11 cleaves gasdermin D for non-canonical inflammasome signalling. Nature *526*, 666-671. 10.1038/nature15541.
12. Shi, J., Zhao, Y., Wang, K., Shi, X., Wang, Y., Huang, H., Zhuang, Y., Cai, T., Wang, F., and Shao, F. (2015). Cleavage of GSDMD by inflammatory caspases determines pyroptotic cell death. Nature *526*, 660-665. 10.1038/nature15514.
13. Ding, J., Wang, K., Liu, W., She, Y., Sun, Q., Shi, J., Sun, H., Wang, D.C., and Shao, F. (2016). Pore-forming activity and structural autoinhibition of the gasdermin family. Nature *535*, 111-116. 10.1038/nature18590.
14. Kenney, A.D., Li, Z., Bian, Z., Zhou, X., Li, H., Whitson, B.A., Tan, T., Cai, C., Ma, J., and Yount, J.S. (2021). Recombinant MG53 Protein Protects Mice from Lethal Influenza Virus Infection. Am J Respir Crit Care Med *203*, 254-257. 10.1164/rccm.202007-2908LE.

15. Sermersheim, M., Kenney, A.D., Lin, P.H., McMichael, T.M., Cai, C., Gumpper, K., Adesanya, T.M.A., Li, H., Zhou, X., Park, K.H., et al. (2020). MG53 suppresses interferon-beta and inflammation via regulation of ryanodine receptor-mediated intracellular calcium signaling. Nat Commun *11*, 3624. 10.1038/s41467-020-17177-6.
16. Mulvihill, E., Sborgi, L., Mari, S.A., Pfreundschuh, M., Hiller, S., and Muller, D.J. (2018). Mechanism of membrane pore formation by human gasdermin-D. EMBO J *37*. 10.15252/embj.201798321.
17. Liu, X., Zhang, Z., Ruan, J., Pan, Y., Magupalli, V.G., Wu, H., and Lieberman, J. (2016). Inflammasome-activated gasdermin D causes pyroptosis by forming membrane pores. Nature *535*, 153-158. 10.1038/nature18629.
18. Gaidt, M.M., and Hornung, V. (2016). Pore formation by GSDMD is the effector mechanism of pyroptosis. EMBO J *35*, 2167-2169. 10.15252/embj.201695415.
19. Aglietti, R.A., Estevez, A., Gupta, A., Ramirez, M.G., Liu, P.S., Kayagaki, N., Ciferri, C., Dixit, V.M., and Dueber, E.C. (2016). GsdmD p30 elicited by caspase-11 during pyroptosis forms pores in membranes. Proc Natl Acad Sci U S A *113*, 7858-7863. 10.1073/pnas.1607769113.
20. Bent, R., Moll, L., Grabbe, S., and Bros, M. (2018). Interleukin-1 Beta-A Friend or Foe in Malignancies? Int J Mol Sci *19*. 10.3390/ijms19082155.
21. Vecchie, A., Bonaventura, A., Toldo, S., Dagna, L., Dinarello, C.A., and Abbate, A. (2021). IL-18 and infections: Is there a role for targeted therapies? J Cell Physiol *236*, 1638-1657. 10.1002/jcp.30008.
22. Sollberger, G., Choidas, A., Burn, G.L., Habenberger, P., Di Lucrezia, R., Kordes, S., Menninger, S., Eickhoff, J., Nussbaumer, P., Klebl, B., et al. (2018). Gasdermin D plays a vital role in the generation of neutrophil extracellular traps. Sci Immunol *3*. 10.1126/sciimmunol.aar6689.
23. Chen, X., Liu, S., Goraya, M.U., Maarouf, M., Huang, S., and Chen, J.L. (2018). Host Immune Response to Influenza A Virus Infection. Front Immunol *9*, 320. 10.3389/fimmu.2018.00320.
24. Ma, Y., Zhang, Y., and Zhu, L. (2021). Role of neutrophils in acute viral infection. Immun Inflamm Dis *9*, 1186-1196. 10.1002/iid3.500.
25. Tate, M.D., Deng, Y.M., Jones, J.E., Anderson, G.P., Brooks, A.G., and Reading, P.C. (2009). Neutrophils ameliorate lung injury and the development of severe disease during influenza infection. J Immunol *183*, 7441-7450. 10.4049/jimmunol.0902497.
26. Tate, M.D., Brooks, A.G., and Reading, P.C. (2008). The role of neutrophils in the upper and lower respiratory tract during influenza virus infection of mice. Respir Res *9*, 57. 10.1186/1465-9921-9-57.
27. Tate, M.D., Brooks, A.G., Reading, P.C., and Mintern, J.D. (2012). Neutrophils sustain effective CD8(+) T-cell responses in the respiratory tract following influenza infection. Immunol Cell Biol *90*, 197-205. 10.1038/icb.2011.26.
28. Tate, M.D., Ioannidis, L.J., Croker, B., Brown, L.E., Brooks, A.G., and Reading, P.C. (2011). The role of neutrophils during mild and severe influenza virus infections of mice. PLoS One *6*, e17618. 10.1371/journal.pone.0017618.
29. Narasaraju, T., Yang, E., Samy, R.P., Ng, H.H., Poh, W.P., Liew, A.A., Phoon, M.C., van Rooijen, N., and Chow, V.T. (2011). Excessive neutrophils and neutrophil extracellular traps contribute to acute lung injury of influenza pneumonitis. Am J Pathol *179*, 199-210. 10.1016/j.ajpath.2011.03.013.
30. Sugamata, R., Dobashi, H., Nagao, T., Yamamoto, K., Nakajima, N., Sato, Y., Aratani, Y., Oshima, M., Sata, T., Kobayashi, K., et al. (2012). Contribution of neutrophil-derived myeloperoxidase in the early phase of fulminant acute respiratory distress syndrome induced by influenza virus infection. Microbiol Immunol *56*, 171-182. 10.1111/j.1348-0421.2011.00424.x.

31. Zhu, L., Liu, L., Zhang, Y., Pu, L., Liu, J., Li, X., Chen, Z., Hao, Y., Wang, B., Han, J., et al. (2018). High Level of Neutrophil Extracellular Traps Correlates With Poor Prognosis of Severe Influenza A Infection. J Infect Dis *217*, 428-437. 10.1093/infdis/jix475.
32. Xu, T., Qiao, J., Zhao, L., Wang, G., He, G., Li, K., Tian, Y., Gao, M., Wang, J., Wang, H., and Dong, C. (2006). Acute respiratory distress syndrome induced by avian influenza A (H5N1) virus in mice. Am J Respir Crit Care Med *174*, 1011-1017. 10.1164/rccm.200511-1751OC.
33. Lund, M.E., To, J., O'Brien, B.A., and Donnelly, S. (2016). The choice of phorbol 12-myristate 13-acetate differentiation protocol influences the response of THP-1 macrophages to a pro-inflammatory stimulus. J Immunol Methods *430*, 64-70. 10.1016/j.jim.2016.01.012.
34. Moltedo, B., Li, W., Yount, J.S., and Moran, T.M. (2011). Unique type I interferon responses determine the functional fate of migratory lung dendritic cells during influenza virus infection. PLoS Pathog *7*, e1002345. 10.1371/journal.ppat.1002345.
35. Ruifrok, A.C., and Johnston, D.A. (2001). Quantification of histochemical staining by color deconvolution. Anal Quant Cytol Histol *23*, 291-299.
36. Kenney, A.D., Aron, S.L., Gilbert, C., Kumar, N., Chen, P., Eddy, A., Zhang, L., Zani, A., Vargas-Maldonado, N., Speaks, S., et al. (2022). Influenza virus replication in cardiomyocytes drives heart dysfunction and fibrosis. Sci Adv *8*, eabm5371. 10.1126/sciadv.abm5371.
37. Kenney, A.D., Zani, A., Kawahara, J., Eddy, A.C., Wang, X.L., Mahesh, K.C., Lu, M., Thomas, J., Kohlmeier, J.E., Suthar, M.S., et al. (2023). Interferon-induced transmembrane protein 3 (IFITM3) limits lethality of SARS-CoV-2 in mice. EMBO Rep, e56660. 10.15252/embr.202256660.
38. Ritchie, M.E., Phipson, B., Wu, D., Hu, Y., Law, C.W., Shi, W., and Smyth, G.K. (2015). limma powers differential expression analyses for RNA-sequencing and microarray studies. Nucleic Acids Res *43*, e47. 10.1093/nar/gkv007.
39. Gillespie, M., Jassal, B., Stephan, R., Milacic, M., Rothfels, K., Senff-Ribeiro, A., Griss, J., Sevilla, C., Matthews, L., Gong, C., et al. (2022). The reactome pathway knowledgebase 2022. Nucleic Acids Res *50*, D687-D692. 10.1093/nar/gkab1028.
40. Franzen, O., Gan, L.M., and Bjorkegren, J.L.M. (2019). PanglaoDB: a web server for exploration of mouse and human single-cell RNA sequencing data. Database (Oxford) *2019*. 10.1093/database/baz046.
41. Miller, M.D., Wilson, S.D., Dorf, M.E., Seuanez, H.N., O'Brien, S.J., and Krangel, M.S. (1990). Sequence and chromosomal location of the I-309 gene. Relationship to genes encoding a family of inflammatory cytokines. J Immunol *145*, 2737-2744.
42. Haque, N.S., Zhang, X., French, D.L., Li, J., Poon, M., Fallon, J.T., Gabel, B.R., Taubman, M.B., Koschinsky, M., and Harpel, P.C. (2000). CC chemokine I-309 is the principal monocyte chemoattractant induced by apolipoprotein(a) in human vascular endothelial cells. Circulation *102*, 786-792. 10.1161/01.cir.102.7.786.
43. Orzalli, M.H., Smith, A., Jurado, K.A., Iwasaki, A., Garlick, J.A., and Kagan, J.C. (2018). An Antiviral Branch of the IL-1 Signaling Pathway Restricts Immune-Evasive Virus Replication. Mol Cell *71*, 825-840 e826. 10.1016/j.molcel.2018.07.009.
44. Aarreberg, L.D., Esser-Nobis, K., Driscoll, C., Shuvarikov, A., Roby, J.A., and Gale, M., Jr. (2019). Interleukin-1beta Induces mtDNA Release to Activate Innate Immune Signaling via cGAS-STING. Mol Cell *74*, 801-815 e806. 10.1016/j.molcel.2019.02.038.
45. Gramegna, A., Amati, F., Terranova, L., Sotgiu, G., Tarsia, P., Miglietta, D., Calderazzo, M.A., Aliberti, S., and Blasi, F. (2017). Neutrophil elastase in bronchiectasis. Respir Res *18*, 211. 10.1186/s12931-017-0691-x.

46. Peschke, T., Bender, A., Nain, M., and Gemsa, D. (1993). Role of macrophage cytokines in influenza A virus infections. Immunobiology *189*, 340-355. 10.1016/s0171-2985(11)80365-7.
47. Cline, T.D., Beck, D., and Bianchini, E. (2017). Influenza virus replication in macrophages: balancing protection and pathogenesis. J Gen Virol *98*, 2401-2412. 10.1099/jgv.0.000922.
48. Kalil, A.C., and Thomas, P.G. (2019). Influenza virus-related critical illness: pathophysiology and epidemiology. Crit Care *23*, 258. 10.1186/s13054-019-2539-x.
49. Force, A.D.T., Ranieri, V.M., Rubenfeld, G.D., Thompson, B.T., Ferguson, N.D., Caldwell, E., Fan, E., Camporota, L., and Slutsky, A.S. (2012). Acute respiratory distress syndrome: the Berlin Definition. JAMA *307*, 2526-2533. 10.1001/jama.2012.5669.
50. Grommes, J., and Soehnlein, O. (2011). Contribution of neutrophils to acute lung injury. Mol Med *17*, 293-307. 10.2119/molmed.2010.00138.
51. Xie, J., Zhu, C.L., Wan, X.J., Zhao, Z.Z., Meng, Y., Li, P., Guo, Y., Liu, Q., Bian, J.J., Deng, X.M., and Wang, J.F. (2023). GSDMD-mediated NETosis promotes the development of acute respiratory distress syndrome. Eur J Immunol *53*, e2250011. 10.1002/eji.202250011.
52. Bauer, R.N., Brighton, L.E., Mueller, L., Xiang, Z., Rager, J.E., Fry, R.C., Peden, D.B., and Jaspers, I. (2012). Influenza enhances caspase-1 in bronchial epithelial cells from asthmatic volunteers and is associated with pathogenesis. J Allergy Clin Immunol *130*, 958-967 e914. 10.1016/j.jaci.2012.07.013.
53. Ichinohe, T., Lee, H.K., Ogura, Y., Flavell, R., and Iwasaki, A. (2009). Inflammasome recognition of influenza virus is essential for adaptive immune responses. J Exp Med *206*, 79-87. 10.1084/jem.20081667.
54. Wurzer, W.J., Planz, O., Ehrhardt, C., Giner, M., Silberzahn, T., Pleschka, S., and Ludwig, S. (2003). Caspase 3 activation is essential for efficient influenza virus propagation. EMBO J *22*, 2717-2728. 10.1093/emboj/cdg279.
55. Galvin, H.D., and Husain, M. (2019). Influenza A virus-induced host caspase and viral PA-X antagonize the antiviral host factor, histone deacetylase 4. J Biol Chem *294*, 20207-20221. 10.1074/jbc.RA119.010650.
56. Porritt, R.A., and Hertzog, P.J. (2015). Dynamic control of type I IFN signalling by an integrated network of negative regulators. Trends Immunol *36*, 150-160. 10.1016/j.it.2015.02.002.
57. Guo, X.J., and Thomas, P.G. (2017). New fronts emerge in the influenza cytokine storm. Semin Immunopathol *39*, 541-550. 10.1007/s00281-017-0636-y.
58. Teijaro, J.R. (2015). The role of cytokine responses during influenza virus pathogenesis and potential therapeutic options. Curr Top Microbiol Immunol *386*, 3-22. 10.1007/82_2014_411.